Surface-plasmon-enhanced fluorescence from periodic quantum dot arrays through distance control using biomolecular linkers

To cite this article: Melvin T Zin *et al* 2009 *Nanotechnology* **20** 015305

Nanotechnology **20** (2009) 015305 (7pp) doi:10.1088/0957-4484/20/1/015305

Surface-plasmon-enhanced fluorescence from periodic quantum dot arrays through distance control using biomolecular linkers

Melvin T Zin[1,2], Kirsty Leong[3], Ngo-Yin Wong[1], Hong Ma[1], Mehmet Sarikaya[1] and Alex K-Y Jen[1,3,4]

[1] Department of Materials Science and Engineering, University of Washington, Seattle, WA 98195, USA
[2] 3M Corporate Research Analytical Laboratory, 3M Center, St Paul, MN 55144, USA
[3] Department of Chemistry, University of Washington, Seattle, WA 98195, USA

E-mail: ajen@u.washington.edu

Received 25 August 2008, in final form 7 October 2008
Published 5 December 2008
Online at stacks.iop.org/Nano/20/015305

Abstract
We have developed a protein-enabled strategy to fabricate quantum dot (QD) nanoarrays where up to a 15-fold increase in surface-plasmon-enhanced fluorescence has been achieved. This approach permits a comprehensive control both laterally (via lithographically defined gold nanoarrays) and vertically (via the QD–metal distance) of the collectively behaving assemblies of QDs and gold nanoarrays by way of biomolecular recognition. Specifically, we demonstrated the spectral tuning of plasmon resonant metal nanoarrays and self-assembly of protein-functionalized QDs in a stepwise fashion with a concomitant incremental increase in separation from the metal surface through biotin–streptavidin spacer units.

S Supplementary data are available from stacks.iop.org/Nano/20/015305

(Some figures in this article are in colour only in the electronic version)

1. Introduction

Over the past decade, there has been an increasing coordination between materials science and biological science at the nanometer scale [1–3]. This endeavor is driven by the prospect of harnessing unique advantages that are inherent in both biomolecules and inorganic nanostructures and the fact that these two classes of material are on a comparable length scale. With recent advances in genetic engineering [4] and chemical synthesis [5–7], it is now possible to tailor the characteristics of these two classes of material with a great level of control. Hybrid nanoassemblies made from inorganic nanostructures and biomolecules serve as versatile nanocomposites with a range of surface functionalities as well as optical and electronic properties that arise from co-operative interactions. Of peculiar utility in nanobiotechnology are integrated systems of designed peptides/proteins, metal nanostructures and quantum dots (QDs) [8, 9]. Interesting opportunities emerge in mixed nanoassemblies where peptides/proteins can impart self-assembly and biomolecular recognition capabilities to the overall construct while the plasmonic properties of metal nanoarrays [10–12] can be engineered to manipulate the emission properties of QDs [13] for creating ultra-sensitive sensors where a change in fluorescence indicates an occurrence of a specific binding event. Despite the importance of fluorescence labeling in protein diagnostics, research in the use of peptides/proteins in plasmon-enhanced fluorescence has been limited. So far, most hybrid nanoassemblies with plasmon-modulated fluorescence are DNA-based systems [14–18], and it is critical to develop protein-based systems as an alternate technology.

We demonstrate here the peptide-mediated fabrication of QD arrays where up to a 15-fold increase in surface-plasmon-enhanced fluorescence has been achieved. This

[4] Author to whom any correspondence should be addressed.

result, to the best of our knowledge, represents the highest fluorescence enhancement from hybrid nanoassemblies based on biomolecules.

This work differs significantly from earlier reports on biophotonic conjugates in several important aspects. First, it is a protein-enabled strategy. As nanoscale building blocks, proteins are structurally and chemically versatile. There are 20 commonly occurring amino acids with more rare variants and many more synthetic analogues for proteins; moreover, functional moieties (e.g., amines) appended to amino acids can participate in chemical reactions. As a result, protein-derived constructs may find a wide spectrum of applications in nanobiotechnology. Second, we show a proof of concept to rationally optimize plasmon-modulated fluorescence through the spectral tuning of plasmon resonant metal nanoarrays. Third, the use of QDs instead of organic dyes is appealing due to their inherent advantages such as excellent photochemical stability, high quantum yields and spectral tunability. Their broad absorption band, for instance, permits flexibility in spectral overlapping to induce near-field effects. Fourth, template-guided immobilization of protein-functionalized QDs using designed peptides and protein spacers offers a universal platform to generate hybrid nanoassemblies with high specificity and nanoscale (about 5 nm) precision; well-defined hybrid nanoassemblies as large as ∼20–30 nm in height were demonstrated in a modular manner. Lastly, our approach facilitates a direct quantitative comparison of emission from a series of QD arrays on a given sample as well as from multiple experiments acquired simultaneously.

2. Experimental details

2.1. Fabrication of plasmon resonant gold nanoarrays

Electron-beam lithography (EBL) was performed using a field emission scanning electron microscope (SEM; FEI Sirion, Hillsboro, OR) that has been equipped a nanolithography system. A nanometer pattern generation system (NPGS), developed by JC Nabity Lithography System (Bozeman, MT), was used to design and direct-write nanoarrays. (See figure S-1 (available at stacks.iop.org/Nano/20/015305) for a schematic illustration of the fabrication procedure and structural parameters of metal nanoarrays.) The resolution of the nanolithography system is approximately 20 nm. Prior to EBL, Si wafers were fractured into small substrates and cleaned in a two-step procedure: (i) piranha etch, 3:1 H_2SO_4:H_2O_2(30%) for 1 h; (ii) base treatment, 5:1:1 H_2O:NH_4OH:H_2O_2(30%) with sonication for 1 h. Thin films (50–80 nm) of polymethyl methacrylate (PMMA; 950k; diluted in chlorobenzene) resist were spin-coated on Si(001) substrates, annealed at 180 °C on a hot plate for 2 min to improve the film uniformity, and then exposed to an electron beam at an accelerating voltage of 30 keV. After the electron-beam exposure, samples were developed in a 1:3 mixture of methyl-isobutylketone/isopropanol (MIBK/IPA) at room temperature for ∼30 s and baked at 90 °C in a vacuum oven for 30 min. The samples were checked by SEM to assess the integrity of nanopatterned PMMA films before the metalization process. Metal was deposited onto nanopatterned PMMA films by electron-beam evaporation (SEC 6000, CHA Industries) under a high vacuum with base pressure of $\sim 1 \times 10^{-6}$ Torr. For stronger adhesion of gold to silicon, 1 nm of chromium was used. The deposited thickness and deposition rate were measured by a quartz crystal microbalance (QCM). The deposition rate was maintained at ~ 0.1 nm s^{-1} to achieve high-quality gold nanostructures with smooth surfaces. In the lift-off step, gold nanoarrays were obtained by dissolving the PMMA resist in acetone overnight (∼12 h). To ensure the complete removal of PMMA, samples were treated as follows: (i) thorough rinsing in acetone and IPA; (ii) brief immersion in a piranha solution for 3 min; (iii) oxygen plasma etch for 30 min. It is critical that the PMMA resist is entirely stripped from the substrate in order for the molecular linkers to self-assemble specifically onto metal nanoarrays. Empirical evidence suggests that PMMA interferes with the self-assembly protocol by binding with peptides and streptavidin molecules, presumably through van der Waals and electrostatic interactions. This often leads to non-specific adsorption of molecular linkers.

2.2. Assembly of molecular linkers

The 14-amino-acid-long (MHGKTQATSGTIQS) gold-binding peptide (GBP), referred to as GBP1, was combinatorially selected and further engineered to bind with gold surfaces through surface recognition. In this study, biotin (bio) was incorporated to 3-repeat GBP1 (bio–3RGBP1, bio–$[MHGKTQATSGTIQS]_3$) at the *N*-terminus to create a bifunctional biomolecular construct which serves as a binder for specific adsorption to the gold substrate as well as a receptor for controlling the self-assembly of streptavidin (SA)-functionalized CdSe–ZnS QDs (SA-QDs) through bio–SA binding. The assembly protocol consists of the binding of bio–3RGBP1 onto the gold nanoarrays, followed by a sequential attachment of spacer units made of streptavidin and 1-4-dibiotinylbutane. It is carried out by immersing samples into 2 ml solutions of respective molecular linkers for specific durations. Immobilization of bio–3RGBP1 onto the gold nanoarrays was allowed for 2 h to ensure a uniform well-packed foundation layer. Onto biotin-functionalized metal nanostructures, streptavidin and 1-4-dibiotinylbutane were sequentially attached using the reaction time of 35 min between each attachment. It is critical to completely remove excess molecular linkers after each attachment to accomplish reproducible spacer units of well-defined lengths. This is done by (i) successive washing in phosphate buffer (∼3 min) and water (∼3 min), and (ii) gentle sonication in water (∼1 min). The presence of residual molecular linkers from a previous step detrimentally affects the subsequent step by lowering the efficiency of specific binding.

2.3. Assembly of CdSe–ZnS quantum dots

As the final step in the assembly protocol, SA-QDs were attached onto biotinylated linkers through bio–SA binding. The sample was positioned in a Petri dish and incubated for

45 min with QDs by pipetting an SA-QD diluted solution (50 μl) onto a nanopatterned area ($\sim$5 $\times$ 5 mm^2) on the substrate. For a reliable comparison, in preparing control samples on planar and nanopatterned gold surfaces, the same volume (50 μl) of QD solution was pipetted onto a region of equal area ($\sim$5 $\times$ 5 mm^2) on either a planar or nanopatterned gold surface. During QD assembly, the Petri dish was enclosed with a lid to provide stable environmental conditions. A few droplets of water were placed besides the sample to prevent the evaporation of the QD solution. This minimizes minor changes in the local concentration of the QD solution.

2.4. Measurement of linker lengths

Atomic force microscopy (AFM) measurements were carried out in air under ambient conditions (about 40%–50% relative humidity, 25 °C) on a Digital Instruments Nanoscope IIIa Multimode AFM (Veeco Inc., Santa Barbara, CA) using tapping mode. Silicon probes (Veeco Inc., Santa Barbara, CA) that have an effective radius of curvature of $\sim$10 nm were used. The heights of molecular linkers were experimentally measured relative to the height of 11-mercaptoundecyl-tri(ethylene glycol)-alcohol (OEG; 1 mM ethanolic solution) self-assembled monolayers (see figure S-2 (available at stacks.iop.org/Nano/20/015305)). This is accomplished by backfilling of linkers into 2 μm hole arrays generated by microcontact printing of OEG molecules, followed by cross-sectional profile analysis to measure the relative difference in heights between patterned OEG regions and linker regions.

2.5. Optical characterization

Optical microscopy and spectroscopy were performed on an inverted microscope (Eclipse TE2000-U, Nikon) equipped with a true-color digital camera and a spectrometer (USB2000, Ocean Optics). Unpolarized white light illumination by a 120 W metal halide lamp (EXFO X-Cite 120) was used as an excitation source. Measurements were done with a low-loss fiber optic cable with 50 μm core diameter (Thorlabs, Newton, NJ). The charge coupled device (CCD) detector has a 200–1100 nm range and a sensitivity of 41 photons/count at 600 nm. To check for the homogeneity and reproducibility of QD emission, samples were mounted on a translation stage (MS-2000 XYZ Automated Stage, Eugene, OR) and the PL spectra were acquired in 1 μm steps within each pattern. The scattering spectrum is taken first from a nanopatterned area and then from a region of the sample without any gold nanopillars (i.e., bare substrate). The background scattering spectrum is subtracted from the scattering spectrum of the metal nanoarrays. The wavelength dependence of the excitation source, optics, and CCD detector is removed by normalizing the measured scattering spectrum from the metal nanostructures to that from a non-resonant surface. Spectralon®, purchased from Labsphere (Laguna Niguel, CA), was used as a reflectance surface.

3. Results and discussion

One of the key aspects of this research is the rational optimization of plasmon-modulated fluorescence by properly matching the resonant spectra of metal nanoarrays with the absorption/emission spectra of fluorophores. Figure 1 shows plasmon resonant gold nanoarrays for coupling with QDs. We concentrate here on gold to demonstrate a proof of concept of spectral tuning because of its stability and strong scattering of light in the visible frequencies [19]. Additionally, it allows specific adsorption of gold-binding polypeptide (bio–3RGBP1) as will be discussed below. The use of silver nanoarrays, which show stronger plasmon resonances but are unstable and easily deformable, is deferred to a future study. A sketch of the gold nanopillars in a square lattice (figure 1 inset) defines the structural parameters that were varied systematically: the diameter (D) and tip-to-tip distance (d_{tt}). By keeping the height fixed at 50 nm, gold nanopillars of three sizes (D = 50, 100, 200 nm) were periodically ordered at four grating constants (d_{tt} = 200, 150, 100, 50 nm) to produce nine unique arrangements. As labeled in figure 1, the gold nanoarrays are designated as 1.1 (D = 50 nm; d_{tt} = 200 nm), 1.2 (D = 50 nm; d_{tt} = 150 nm), 1.3 (D = 50 nm; d_{tt} = 100 nm), 1.4 (D = 50 nm; d_{tt} = 50 nm), 2.1 (D = 100 nm; d_{tt} = 200 nm), 2.2 (D = 100 nm; d_{tt} = 150 nm), 2.3 (D = 100 nm; d_{tt} = 100 nm), 3.1 (D = 200 nm; d_{tt} = 200 nm), and 3.2 (D = 200 nm; d_{tt} = 150 nm). All patterns were fabricated on the same sample—each pattern occupied 10 $\times$ 10 μm^2 and was repeated three times to ensure reproducibility and acquire a larger data set.

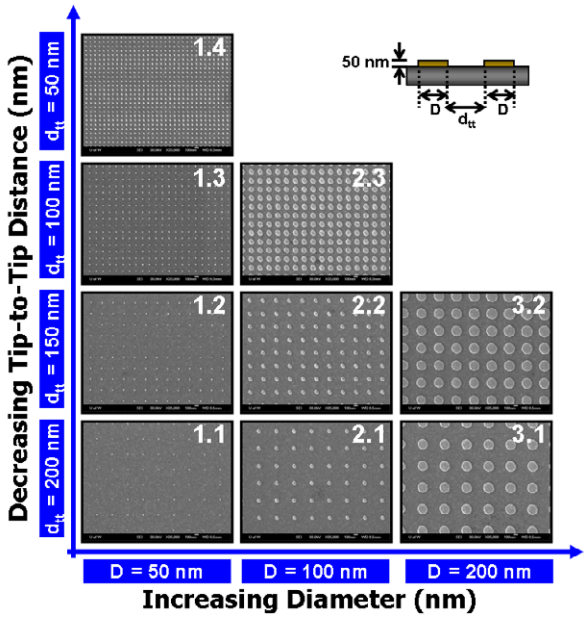

Figure 1. SEM images of gold nanoarrays. EBL readily allows the precision control of the size and interspacing of the gold nanopillars, ideal for the spectral tuning of plasmon resonant gold nanoarrays and study of their electromagnetic interactions. By keeping the height constant (h = 50 nm), gold nanopillars of three sizes (D = 50, 100, 200 nm) were periodically ordered at four grating constants (d_{tt} = 200, 150, 100, 50 nm) to produce nine unique arrangements. Each pattern occupied 10 $\times$ 10 μm^2 and was repeated three times to ensure reproducibility and acquire a larger data set. All patterns were fabricated on the same sample.

Table 1 summarizes the physical and optical characteristics of the metal nanoarrays. To account for the differences in

Table 1. Structural parameters of the gold nanoarrays.

	Array	Gold nanopillar dimensions D (nm)	d_{tt} (nm)	Area fill factor	LSPR peak λ_{max} (nm)
1	1.1	50	200	0.031	IR
2	1.2	50	150	0.049	IR
3	1.3	50	100	0.087	IR
4	1.4	50	50	0.196	IR
5	2.1	100	200	0.087	440.3
6	2.2	100	150	0.126	488.1
7	2.3	100	100	0.196	580.6
8	3.1	200	200	0.196	546.2
9	3.2	200	150	0.256	549.0

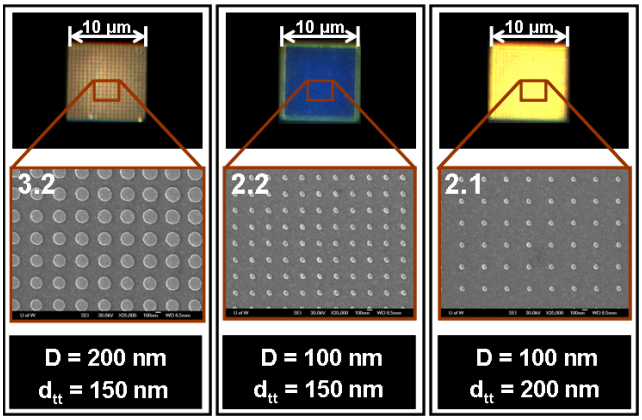

Figure 2. Dark-field images of gold nanoarrays. Precision control of the size and interspacing of the gold nanopillars leads to metal nanoarrays with distinct light scattering properties.

the packing density of the gold nanopillars due to differences in D and d_{tt}, it is necessary to calculate the area fill factor of each pattern. The area fill factor is defined as the ratio $\pi(D/2)^2/(D + d_{tt})^2$. Normalizing the fluorescence intensity measurements by area fill factor therefore removes the higher contribution to intensity of QD emission from arrays with smaller tip-to-tip spacing (which results in a larger percentage of gold surface per unit area). This allows for a head-to-head comparison of surface-plasmon-enhanced photoluminescence (PL) from QD nanoarrays.

Plasmon excitations in metal nanostructures produce extinction spectra that depend sensitively on their shape and size as well as the dielectric properties of their surrounding medium and the material from which they are made [19]. For periodically ordered metal nanostructures, the resonance phenomenon is additionally complicated by electromagnetic (EM) interaction between individual nanostructures [20, 21]. Two types of optical communication can be distinguished in a regular 2D configuration: near-field coupling and far-field (dipolar) interaction. Due to the short range of EM near-fields in the order of tens of nm, near-field coupling is especially relevant for 50 nm gold nanoarrays with d_{tt} = 50–100 nm (arrays 1.3 and 1.4) and 100 nm gold nanoarrays with d_{tt} = 100–150 nm (arrays 2.2 and 2.3). Far-field interaction is mediated through the scattered light, which is of dipolar nature for sub-wavelength nanostructures and can be described within a quasi-static model. This manifests in the spectral selective scattering of light as demonstrated in the true-color dark-field images of the gold nanoarrays (figure 2; see also figure S-3 (available at stacks.iop.org/Nano/20/015305)). Gold nanopillars in arrays where d_{tt} is too large to allow near-field coupling radiate collectively via interfering dipolar fields. Nanostructures, similar to nanopillars we are considering here, have been treated as nanowires with a quasi-infinite extension along the symmetry axis [20]. We note that plasmon resonances in nanopillars can only be excited by an EM field oriented perpendicular to the pillar axis—the direction in which the spatial confinement of electrons is provided by the interface of the nanopillar and the adjacent medium; this is in contrast to the case of spherical nanoparticles where plasmon excitation is polarization independent.

Since the nanopillars were fabricated on a silicon substrate (non-transparent) and the nanopatterned areas were close to one another with each pattern occupying only 10 × 10 μm^2, we were not able to obtain the extinction (i.e., absorption plus scattering) or transmission spectra of the gold nanoarrays directly. However, we were able to determine the localized surface-plasmon resonance (LSPR) maxima (λ_{max}) of gold nanoarrays based on scattering [18, 22]. First, the lamp reference scattering spectrum was obtained by measuring the scattered white light from a reflectance surface. Next, the scatting spectrum of each nanoarray was obtained. This nanoarray spectrum divided by the lamp reference spectrum (i.e., the ratio) gave the scattering efficiency, and hence the LSPR, of each nanoarray. It can be seen that the optical properties of 200 nm pillars are independent of the lattice spacings at 200 nm (array 3.1) and 150 nm (array 3.2). This suggests a weak EM interaction between large nanostructures which are not significantly smaller than the light wavelength (i.e., beyond the quasi-static limit). In contrast, the resonant wavelength of 100 nm gold nanoarrays blue-shifts with a decrease in their lattice spacing. This demonstrates the importance of radiative dipolar interaction (which has a $1/d$ dependence on nanoparticle separation) and retardation (which multiplies the dipole field by e^{ikd}) for large grating constants (d_{tt} = 100, 150, 200 nm). We note that 50 nm pillars at all grating constants do not scatter light in the visible frequencies. Indeed, it has been shown that the extinction peaks of arrays of gold nanoparticles with small lattice spacings (relative to their size) red-shifts to IR frequencies [21].

Figure 3 schematically depicts the template-guided immobilization of protein-functionalized QDs at well-defined distances on plasmon resonant gold nanoarrays using designed peptides and protein spacers. The assembly protocol consists of the binding of bio–3RGBP1 onto gold nanoarrays, followed by a sequential attachment of spacer units made of streptavidin and 1-4-dibiotinylbutane. As the final step in the assembly protocol, SA-QDs were attached onto biotinylated linkers through biotin–streptavidin binding. As nanoscale building blocks, SA molecules provide a well-ordered homotetrameric entity with four binding sites, appropriate size (about 5 nm) and high-affinity biomolecular recognition [23]. We accomplished well-defined separation between the metal surface and QDs (defined as S_{Au-QD}) through direct attachment of QDs and

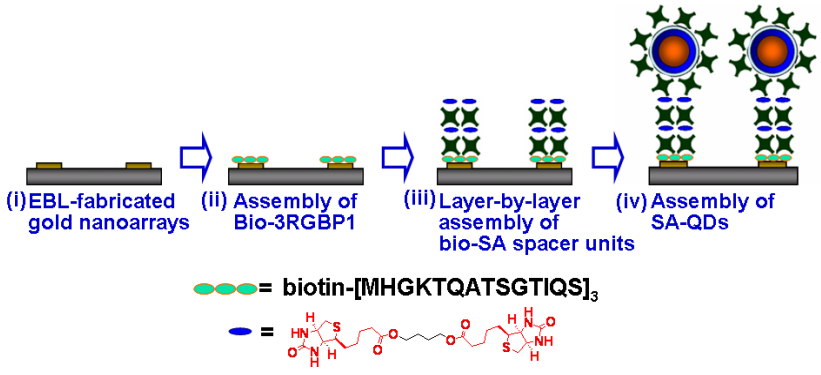

Figure 3. Peptide-mediated fabrication of QD nanoarrays.

by using single and double bio–SA spacer units. These separations positioned the QDs at three spatial locations ($S_{Au-QD} \approx 8.7$, 16.0 and 20.3 nm) within the amplified local EM field of the gold nanopillars where the polarization strength is believed to be drastically different.

The photoluminescence from QD arrays reveals the specificity of coupling QDs onto gold nanopillars with precise alignment (figure 4(a)). The surface-plasmon-enhanced fluorescence can be clearly observed, and the luminescence intensity is homogeneous and reproducible from cell to cell as demonstrated in a series of QD arrays with the highest fluorescence enhancement (array 2.3: $D = 100$ nm, $d_{tt} = 100$ nm, $S_{Au-QD} \approx 16$ nm); the enhancement factor was ~15, relative to the QD emission on a planar gold substrate after normalization over the area fill factor. The self-assembled QDs formed a close-packed, uniform layer, and the extent of aggregation in QD films was not significant. We noticed a slight red-shift in peak position and a narrowing of the linewidth in the solid-state PL spectra, indicating a strong electronic and optical interaction between the QDs and the gold nanopillars (figure 4(b)). In the absence of the gold nanopillars, we did not find a peak position shift or a lineshape change of the emission band even at high solid-state packing densities of QDs because of their monodispersity and their thick SA coating (about 5 nm), which prohibits inter-dot energy transfer. Apparent fluorescence enhancement in coupled exciton–plasmon systems, as observed in figure 4(a), arises from the joint process of incident photon absorption and emission. Incident photons can be absorbed by both metal nanoparticles (i.e., plasmons) and QDs (i.e., excitons). Similarly, photon emission to free space and to the CCD detector can proceed through light scattering aided by the interfering dipole fields of the gold nanoarrays.

Figure 5 compares the area-normalized PL peak intensity plots of different QD arrays. The emission intensity of QD arrays increased sharply as the QD–metal separation (S_{Au-QD}) was increased from ~8.7 nm (figure 5(a)) to ~16.0 nm (figure 5(b)); a 40–50% rise in relative fluorescence enhancement was observed. When the QDs were placed at a greater distance through an additional spacer unit ($S_{Au-QD} \approx$ 20.3 nm), their photoluminescence decreased (figure 5(c)). However, it is interesting to note that the emission intensity of QDs at $S_{Au-QD} \approx 20.3$ nm (figure 5(c)) was still higher

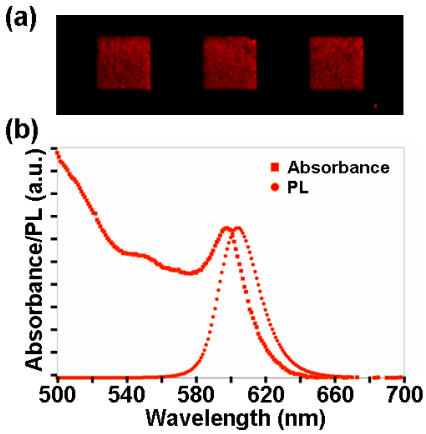

Figure 4. (a) Fluorescence image of a QD nanoarray with the highest fluorescence enhancement (array 2.3: $D = 100$ nm, $d_{tt} = 100$ nm, $S_{Au-QD} \approx 16$ nm); the enhancement factor was ~15, relative to the QD emission on a planar gold substrate after normalization over the area fill factor. (b) Spectral properties of the QDs.

than that at $S_{Au-QD} \approx 8.7$ nm (figure 5(a)). These data suggest that PL quenching is a short-range effect (<5 nm) and is weakened with distance more rapidly than the EM field amplification responsible for the PL enhancement. A similar dependence of QD emission on the separation from the gold surface has been reported where the largest fluorescence enhancement was obtained at ~11.7 nm [24]. We note that although the relative fluorescence enhancement was dependent on the QD–metal separation, the respective photoluminescence trend of a particular QD array remains the same. In contrast to earlier studies based on plasmonic colloidal nanoparticles [24] which are not amenable to lateral structuring in a pattern-wise fashion, the use of a nanopatterned substrate as demonstrated in our approach allows the QD probes to be employed in an array format for possible integration into lab-on-chip sensor applications. Another major disadvantage of systems based on colloidal nanoparticles is the limited degree to which multiple distinct plasmonic resonances can be excited simultaneously on a single substrate—an important feature for multiplexing that is easily achievable as shown in this study by nanofabricating a combinatorial pattern of well-designed periodic arrays with individually unique optical properties.

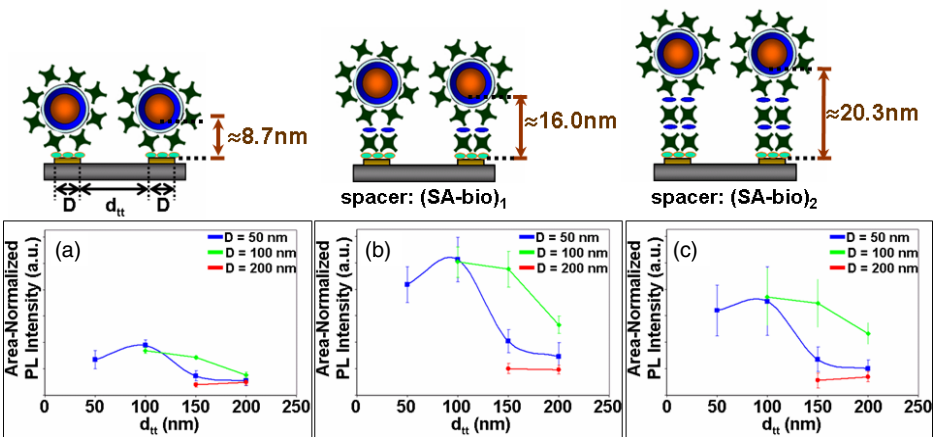

Figure 5. QD nanoarrays with surface-plasmon-enhanced photoluminescence. Area-normalized PL peak intensity from QDs in a particular pattern at different QD–metal distances of 8.7 nm (a), 16.0 nm (b), and 20.3 nm (c). Schematic illustrations show the structure of hybrid nanoassemblies.

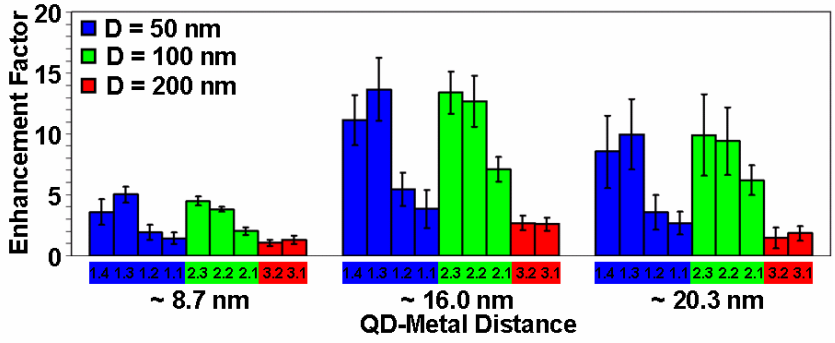

Figure 6. Enhancement factors of the QD nanoarrays. To ensure a reliable normalization, the distance effect was taken into account; QDs are attached onto either gold nanopillars or planar gold substrates using the same linkers and their PL intensities were measured. Enhancement factors were calculated by dividing the PL intensity from QDs in a particular pattern by that from QDs in an unpatterned area.

Figure 6 highlights the effects of the nanoarray (D and d_{tt}) and metal–QD separation (S_{Au-QD}) on the enhancement factor. Among the three sizes of gold nanopillars we studied, 200 nm nanostructures were the least efficient for surface-plasmon-enhanced fluorescence. At a given QD–metal distance, QD emission on 200 nm nanostructures was considerably less than both 100 nm and 50 nm nanostructures. For 200 nm gold nanoarrays, the emission intensity was very similar for an interparticle spacing of 200 nm (array 3.1) and 150 nm (array 3.2), and only moderate enhancement factors were achieved—the highest enhancement factor for 200 nm metal arrays was ∼3 at $S_{Au-QD} \approx 16.0$ nm. This is surprising since one might expect a higher level of surface-plasmon coupling between neighboring nanoparticles when their interparticle spacing is smaller than their size. This suggests a weak optical communication in large metal nanoarrays ($D \geqslant 200$ nm), where nanostructures interact with the excitation light and participate in local EM field enhancement as individual nanostructures, rather than as a collective entity of strongly interacting nanostructures. In contrast, for 100 nm gold nanopillars, when the interparticle spacing was comparable to the nanoparticle size ($d_{tt} = 100$, array 2.3), there was a marked jump in fluorescence enhancement—the highest enhancement factor for 100 nm gold nanoarrays was ∼15 at $S_{Au-QD} \approx 16.0$ nm. Clearly, there is a much stronger optical communication in 100 nm gold nanoarrays. The tip-to-tip distance between them has to be larger ($d_{tt} = 150$ nm, array 2.2; $d_{tt} = 200$ nm, array 2.1) than their diameter ($D = 100$ nm) to see a decrease in fluorescence enhancement. However, the QD emission in 50 nm metal nanoarrays was optimum when the tip-to-tip distance was twice the particle size ($d_{tt} = 100$ nm, array 1.3), and the fluorescence enhancement was diminished when their interparticle spacing became comparable to their diameter ($d_{tt} = 50$ nm, array 1.4). As a result of strongly interacting nanoparticles, a complex plasmon spectrum is generated in dense periodic particle arrays. The resonant band is usually broadened and shifted toward longer wavelengths, presumably to the IR region for 50 nm nanopillars.

For both 50 and 100 nm gold nanoarrays, which exhibit co-operative interactions, the emission intensity is the strongest at $d_{tt} = 100$ nm and $S_{Au-QD} \approx 16.0$ nm. The highest enhancement factor of ∼15 was achieved at $S_{Au-QD} \approx 16.0$ nm in arrays 2.3 ($D = 100$ nm; $d_{tt} = 100$ nm) and 1.3 ($D = 50$ nm; $d_{tt} = 100$ nm). This finding also implies that no significant gain in fluorescence enhancement was obtained by decreasing the size of nanopillars from $D = 100$ to 50 nm.

4. Conclusions

We demonstrate here a protein-based method to construct QD nanoarrays with surface-plasmon-enhanced photoluminescence. In view of optimizing the fluorescence enhancement, there are several key features that make our approach potentially suitable for investigating resonance phenomena in hybrid nanostructures. One advantage is the capability to independently tailor fluorophores (via colloidal synthesis of QDs), and plasmonic template (via lithographic patterning), as well as the emitter–metal distance (via stepwise self-assembly). This opens up different combinations of ways to create optimally integrated systems for a target application. Another advantage is the possibility to engineer hybrid nanoassemblies such that the QDs are sandwiched in the local EM fields of the bottom nanopatterned metal support and the top metal nanoparticle by using the template-directed self-assembly scheme described above. Finally, the unique benefit of genetically engineered polypeptides such as bio–3RGBP1 is their biomolecular recognition for an inorganic compound—potentially specific in terms of its elemental composition, crystallographic orientation, and morphology. This suggests the prospect of potentially using multiple genetically engineered polypeptides (for example, gold-, silver- and platinum-binding peptides) to selectively anchor multiple emitters (for example, red-, green- and blue-emitting QDs) onto plasmonic architectures in a nanoscale proximity to realize simultaneous resonance phenomena—a subject of future projects. A synergetic combination of inorganic nanostructures, peptide-mediated assembly, and lithographic patterning should enable the precise control necessary to produce highly integrated multifunctional hybrid nanoassemblies for a diverse range of nanobiotechnological applications.

Acknowledgments

This project was supported partially by the Bioinspired Materials and Systems Program through the Air Force Office of Scientific Research (US-AFOSR), UW-DURINT (Defense University Research Initiative on Nanotechnology) through the Army Research Office (US-ARO), and the GEMSEC (Genetically Engineered Materials Science and Engineering Center) through the NSF-MRSEC program. A K-Y Jen thanks the Boeing-Johnson Foundation for its support. M T Zin thanks the Center for Nanotechnology for its support. Instrumentation for electron-beam lithography was provided by the Nanotechnology User Facility (NTUF), a member of the National Nanotechnology Infrastructure (NNIN) supported by NSF and the shared experimental facilities of GEMSEC.

References

[1] Seeman N C and Belcher A M 2002 *Proc. Natl Acad. Sci. USA* **99** 6452
[2] Dujardin E and Mann S 2002 *Adv. Mater.* **14** 775
[3] Niemeyer C M 2001 *Angew. Chem. Int. Edn* **40** 4128
[4] Sarikaya M, Tamerler C, Jen A K-Y, Schulten K and Baneyx F 2003 *Nat. Mater.* **2** 577
[5] Burda C, Chen X, Narayanan R and El-Sayed M A 2005 *Chem. Rev.* **105** 1025
[6] Xia Y, Yang P, Sun Y, Wu Y, Mayers B, Gates B, Yin Y, Kim F and Yan H 2003 *Adv. Mater.* **15** 353
[7] Templeton A C, Wuelfing W P and Murray R W 2000 *Acc. Chem. Res.* **33** 27
[8] Oh E, Hong M-Y, Lee D, Nam S-H, Yoon H C and Kim H-S 2005 *J. Am. Chem. Soc.* **127** 3270
[9] Lee J, Govorov A O, Dulka J and Kotov N A 2004 *Nano Lett.* **4** 2323
[10] Wiley B J, Im S H, Li Z-Y, McLellan J M, Siekkinen A and Xia Y 2006 *J. Phys. Chem.* B **110** 15666
[11] Liz-Marzan L M 2006 *Langmuir* **22** 32
[12] Barnes W L, Dereux A and Ebbesen T W 2003 *Nature* **424** 824
[13] Murray C B, Sun S, Gaschler W, Doyle H, Betley T A and Kagan C R 2001 *IBM J. Res. Dev.* **45** 47
[14] Nicewarner-Pena S R, Freeman R G, Reiss B D, He L, Pena D J, Walton I D, Cromer R, Keating C D and Natan M J 2001 *Science* **294** 137
[15] Malicka J, Gryczynski I, Gryczynski Z and Lakowicz J R 2003 *Anal. Biochem.* **315** 57
[16] Dulkeith E, Ringler M, Klar T A, Feldmann J, Munoz Javier A and Parak W J 2005 *Nano Lett.* **5** 585
[17] Lakowicz J R 2006 *Plasmonics* **1** 5
[18] Chen Y, Munechika K and Ginger D S 2007 *Nano Lett.* **7** 690
[19] Kreibig U and Vollmer M 1995 *Optical Properties of Metal Clusters* (Berlin: Springer)
Bohren C F and Huffman D R 1983 *Absorption and Scattering of Light by Small Particles* (New York: Wiley)
[20] Schider G, Krenn J R, Gotschy W, Lamprecht B, Ditlbacher H, Leitner A and Aussenegg F R 2001 *J. Appl. Phys.* **90** 3825
[21] Haynes C L, McFarland A D, Zhao L, Van Duyne R P, Schatz G C, Gunnarsson L, Prikulis J, Kasemo B and Käll M 2003 *J. Phys. Chem.* B **107** 7337
[22] Mock J J, Barbic M, Smith D R, Schultz D A and Schultz S 2002 *J. Chem. Phys.* **116** 6755
[23] Weber P C, Ohlendorf D H, Wendoloski J J and Salem R R 1989 *Science* **243** 85
[24] Kulakovich O, Strekal N, Yaroshevich A, Maskevich S, Gaponenko S, Nabiev I, Woggon U and Artemyev M 2002 *Nano Lett.* **2** 1449